Journal of Engg. Research **Vol. 4 No. (2) June 2016** pp. 151-171

دراسات تجريبية ورقمية على تأثير الضغط الداخل على التدفق المضطرب في المضخات الدوارة

***ينجوان ليو، *ليكين وانج و**زوشاو زو**

*معهد الآلات التشغيلية، جامعة زيجيانج، هانجزوه 310027، الصين

**قسم الهندسة الميكانيكية والاتوماتيكية، جامعة زيجيانج للعلوم التقنية، هانجزوه 310018، الصين

الخلاصة

تهدف هذه الورقة إلى دراسة تأثير الضغط الداخل على التدفقات المضطربة في مضخة دوارة من خلال الدراسات التجريبية والعددية. في الدراسات التجريبية، تم رصد كل من معدل تدفق ومدخل / مخرج ضغوط لحظية مع مختلف الضغوط مدخل. وأظهرت النتائج أن الضغوط الآنية لمدخل / مخرج خفق دوريا والتغيرات التردد يسيطر عليها مع الضغط مدخل. في الدراسات العددية، تم إنشاء نموذج عددي ثنائي الابعاد مبسط لتحليل تدفقات التجويف في مضخة الدوار والتحقق من البيانات التجريبية. وفي الوقت نفسه، تم إدراج تأثيرات الضغط مدخل على الكفاءة الحجمية توزيع حجم فقاعة جزء وتقلبات الضغط. النتائج تظهر أن نموذج عددي مع التجويف أكثر معقولية لمضخة الدوار من النموذج مرحلة واحدة والضغط مدخل يشير إلى وجود تأثير قوي على الخصائص التجويف. تحدث بالضبط، أولا، يقلل من نسبة معدل التدفق الحجمي عند مدخل لكن يزيد عند مخرج مع مدخل الضغط على انخفاض. وعلاوة على ذلك، في ذروة تدفق مدخل إزاحة نسبة معدل الوراء كما يقلل من الضغط مدخل، لكن ذروة نسبة معدل تدفق المخرج لا يعرض أي تأخير. ثانيا، كما يقلل من الضغط مدخل، وجزء حجم الزيادات مرحلة البخار وذروته أيضا إزاحة إلى الوراء. وأخيرا، والضغوط على شفط وتفريغ الجانبين على حد سواء تظهر زيادة مفاجئة في لحظة معينة. لمدخل الضغط العالي، حدوث طفرة الضغط الذي ينشغل فيه الدوارات اثنين تماما مع بعضها البعض، في حين أن وقت للتأخير ضغط طفرة لمدخل الضغط المنخفض.

Experimental and numerical studies on the effect of inlet pressure on cavitating flows in rotor pumps

Yingyuan Liu*,***, Leqin Wang* and Zuchao Zhu**

**Institute of Process Equipment, Zhejiang University, Hangzhou, 310027, China*

***Department of Mechanical Engineering & Automation, Zhejiang Sci-Tech University, Hangzhou, 310018, China*

****Corresponding Author: upc07042128@163.com*

ABSTRACT

This paper aims to investigate the effect of the inlet pressure on cavitating turbulent flows in a rotor pump through experimental and numerical studies. In experimental studies, both the flow rate and the inlet/outlet instantaneous pressures with various inlet pressures were monitored. The results show that the instantaneous pressures of the inlet/outlet pulsate periodically and its dominated frequency changes with the inlet pressure. In numerical studies, a simplified 2D numerical model for analyzing the cavitation flows in the rotor pump was established and verified by the experimental data. Meanwhile, the influences of the inlet pressure on the volumetric efficiency, the distribution of bubble volume fraction and the pressure fluctuation were included. The results present that the numerical model with cavitation is more reasonable for the rotor pump than the single phase model and the inlet pressure indicates a strong influence on cavitation characteristics. Firstly, the volumetric flow rate ratio decreases at the inlet, but increases at the outlet with the inlet pressure on the decrease. Moreover, the peak of the inlet flow rate ratio offsets backward as the inlet pressure decreases, but the peak of outlet flow rate ratio does not display any delay. Secondly, as the inlet pressure decreases, the volume fraction of the vapor phase increases and its peak also offsets backward. Finally, both pressures at suction and the discharge sides present a sudden increase at a certain moment. For a high inlet pressure, the pressure mutation occurs when the two rotors are fully engaged with each other, while the time for pressure mutation delays for a low inlet pressure.

Keywords: Cavitation; dynamic mesh; inlet pressure; rotor pumps.

NOMENCLATURE

$C_{1\varepsilon}$	empirical constant
$C_{2\varepsilon}$	empirical constant
C_{μ}	empirical constant
f_n	rotational frequency (Hz)
F_{con}	condensation coefficient
F_{vap}	evaporation coefficient
$\vec{g}$	gravity acceleration (m^3/s)
k	turbulent kinetic energy (J)
l	liquid phase
L	width of the rotor (mm)
p	pressure (Pa)
p_B	pressure of bubble surface (Pa)
p_{in}	inlet pressure (kPa)
p_{out}	outlet pressure (kPa)
p_v	evaporation pressure of the liquid (Pa)
p_v^*	local value of the evaporation pressure (Pa)
P_{k}	production of turbulence kinetic energy (J)
Q	numerical volume flow rates
Q_{th}	theoretical volume flow rates
R_B	the radius of the bubble (m)
R_c	mass transfer source terms related to the collapse of the vapor bubbles ($kg/(m^3 \cdot s)$)
R_e	mass transfer source terms related to the growth of the vapor bubbles ($kg/(m^3 \cdot s)$)
S	surface tension coefficient of liquid phase
$\vec{u}$	velocity (m/s)
$\overrightarrow{u_v}$	velocity vector of the liquid phase (m/s)
$\overrightarrow{u_l}$	velocity vector of the liquid phase (m/s)
v	vapor phase
v_l	velocity of liquid phase (m/s)

v_{in} velocity of the inlet (m/s)

Z impeller number of the rotor (Z=4)

α volume fraction of the vapor phase

α_{nuc} volume fraction of the nucleation site

σ_k empirical constant

σ_ε empirical constant

ε dissipation rate

ρ density of the mixture (kg/m^3)

ρ_l density of the liquid phase (kg/m^3)

ρ_v density of the vapor phase (kg/m^3)

μ dynamic viscosity of the mixture (Pa s)

μ_t turbulent viscosity (Pa s)

φ rotation angle of two rotors

INTRODUCTION

Rotor pumps are widely adopted in food, beverage, chemical, pharmaceutical and some other industries (Liu *et al*., 2000). For a rotor pump, as shown in Figure 1, two rotors rotate in reverse directions and the fluid is transported from the suction side to the discharge side through the chamber (Huang & Liu, 2009). Due to this special operating principle, rotor pumps have one inherent advantage of self-priming capabilities, which means the pump can start up without pre-irrigation. In other words, the pump works as a vacuum pump initially and then turns into a common water pump, when the air in the suction pipe is exhausted (Huang *et al*., 2014). The self-priming capacity derives from the fact that the rotating rotors can evacuate air in the suction line, producing a local vacuum, and the liquid is compressed into the suction chamber due to the pressure difference. Vacuum at the suction side can cause cavitation, which occurs with the pressure acting on the hydraulic fluid lower than the vapor pressure or the dissolved air separation pressure of the fluid (Totten *et al*., 1998). As we all know, cavitation can cause serious vibration and damage to rotor pumps, which may induce life reduction of the pumps. Thus, cavitation should be taken into consideration in flow analysis of rotor pumps.

In previous studies, the cavitation behavior of rotor pumps is rarely reported. Considering that the rotor pumps are similar to gear pumps, the flow characteristic studies about gear pumps (Erturk *et al*., 2008; Castilla *et al*., 2010; Erturk *et al*., 2011;

Campo *et al*., 2012; Campo *et al*., 2014) may be used as references, where the cavitation has been reported (Campo *et al*., 2012; Campo *et al*., 2014). For example, Campo *et al.* (2012) developed a numerical model for cavitation behavior in gear pumps and analyzed the effect of cavitation on volumetric efficiencies. Meanwhile, the effect of the inlet pressure on volumetric efficiencies was studied using this proposed model (Campo *et al*., 2014). The results show that the inlet pressure has a significant effect on the performance of gear pumps. Seeing that these studies are mainly limited to gear pumps, further investigation on the cavitation behavior of rotor pumps is still needed. Moreover, as far as the best knowledge of the authors, the effect of the inlet pressure on cavitation has not been discussed systematically for rotor pumps. As described above, this paper is mainly to discuss the influence of the inlet pressure on the cavitation flow in rotor pumps through experimental and numerical studies.

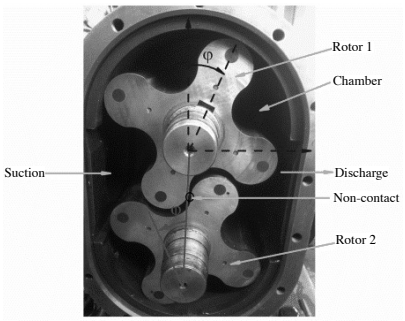

Fig. 1. Schematic diagram of a rotor pump

The structure of the present paper is arranged as follows: Firstly, the cavitation experiment of a rotor pump with different inlet pressures is carried out and the effect of the inlet pressure on flow rates and pressure fluctuations is investigated. Then, a numerical model for cavitation behavior is established and verified by experimental results. Finally, the influence of the inlet pressure on flow characteristics of a rotor pump is reported, including the volumetric efficiency, the volume fraction of the vapor phase, and the pressure fluctuation.

GOVERNING EQUATIONS FOR CAVITATING FLOW

Mixture model

The continuity equation and the momentum equation of the mixture are expressed as Equations (1)-(2), respectively (Fluent A. 14.5, Theory Guide, 2012).

$$\frac{\partial \rho}{\partial t} + \nabla \cdot (\rho \vec{u}) = 0 \tag{1}$$

$$\frac{\partial(\rho\vec{u})}{\partial t}+\nabla\cdot(\rho\vec{u}\vec{u})=-\nabla\cdot\left[(\mu+\mu_t)(\nabla\cdot\vec{u}+\nabla\cdot\vec{u}^T)\right]-\nabla\cdot p+\rho\vec{g}+\nabla\cdot\left[\alpha\rho_v(\vec{u}_v-\vec{u})+(1-\alpha)\rho_l(\vec{u}_l-\vec{u})\right] \quad (2)$$

Turbulence model

In this work, the RNG *k*-*ε* model is employed to close the system of the mixture flow equations. The turbulent kinetic energy and the dissipation rate are shown as Equations (3)-(4) and the turbulent viscosity is given as Equation (5) (Zhang & Khoo, 2014). The values of the five empirical constants in these equations, $C_{1\varepsilon}$, $C_{2\varepsilon}$, C_{μ}, σ_k and σ_ε are 0.0845, 1.45, 1.68, 1.0 and 1.3, respectively.

$$\frac{\partial(\rho k)}{\partial t}+\nabla\cdot\left(\rho\vec{u}k\right)=\mu_t P_k+\nabla\cdot\left(\left(\mu+\mu_t\right)\nabla\cdot k\right)-\rho\varepsilon \quad (3)$$

$$\frac{\partial(\rho\varepsilon)}{\partial t}+\nabla\cdot\left(\rho\vec{u}\varepsilon\right)=C_{1\varepsilon}\left(\frac{\varepsilon}{k}\right)P_k-C_{2\varepsilon}\rho\left(\frac{\varepsilon^2}{k}\right)+\nabla\cdot\left(\left(\mu+\mu_t\right)\nabla\cdot\varepsilon\right) \quad (4)$$

$$\mu_t=\rho C_\mu\frac{k^2}{\varepsilon} \quad (5)$$

Cavitation model

When cavitation occurs, the liquid-vapor mass transformation (evaporation and condensation) is governed by the vapor transport equation (Equation (6)) (Zhang *et al.*, 2010).

$$\frac{\partial}{\partial t}(\alpha\rho_v)+\nabla\cdot\left(\alpha\rho_v\vec{u_v}\right)=R_e-R_c \quad (6)$$

The growth and collapse of vapor bubbles are governed by the Rayleigh-Plesset equation (Brennen, 1995) (Equation (7)). Neglecting the second-order terms and the surface tension force, the bubble dynamic equation is simplified as Equation (8) (Mejri *et al.*, 2006).

$$R_B\frac{D^2R_B}{Dt^2}+\frac{3}{2}\left(\frac{DR_B}{Dt}\right)^2+\frac{4\nu_l}{R_B}R_B+\frac{2S}{\rho_l R_B}=\left(\frac{p_B-p}{\rho_l}\right) \quad (7)$$

$$\frac{DR_B}{Dt}=\sqrt{\frac{2}{3}\frac{p_B-p}{\rho_l}} \quad (8)$$

The equations of mass exchange rates, proposed by Zwart-Gerber-Belamri (Zwart *et al.*, 2004) are employed and the equations for vaporization and condensation are given as follows:

$$R_e = F_{vap}\frac{3\alpha_{nuc}(1-\alpha)\rho_v}{R_B}\sqrt{\frac{2}{3}\frac{p_v - p}{\rho_l}} \tag{9}$$

$$R_c = F_{con}\frac{3\alpha_{nuc}\alpha\rho_v}{R_B}\sqrt{\frac{2}{3}\frac{p_v - p}{\rho_l}} \tag{10}$$

Taking the turbulent pressure fluctuations into consideration, the evaporation pressure p_v should be corrected by Equation (11) (Liu *et al*., 2009).

$$p_v = p_v^* + \frac{1}{2}(0.39\rho k) \tag{11}$$

where, p_v^* is the local evaporation pressure. For the medium discussed below (water), the local evaporation pressure is 3169Pa (absolute pressure) at room temperature (300K).

CAVITATION EXPERIMENTS OF A ROTOR PUMP

Test configurations

In order to verify the computational results, a test system is established (Figure 2). The whole test system is mainly composed of three components: pump system, pipe system and data acquisition system (not shown in Figure 2). For the pump and pipe systems, water is pumped through the pipe system and finally returns to the water tank, forming a circulation system. The pump is driven by a 2-pole 11 kW induction inverter motor and the rotating speed of the pump is controlled by the inverter steplessly ranging from 0r/min to 720r/min. For the data acquisition system, two absolute pressure sensors are located at the inlet and the outlet of the pump, respectively. Both the pressure sensors are rangesing from 0 to 0.2MPa and the accuracies of both the pressure sensors are 2.5%. Thus, the absolute errors of the pressure sensors at the inlet and the outlet are both 0.005MPa. In addition, the response frequency of the pressure sensors is 1000Hz. The output signals of both pressure sensors are the electric current signals ranging from 4 to 20mA. For convenience, the pressure sensors should cascade a resistance of 250Ω and the received signals change to voltage signals ranging from 1 to 5V. Combining the ranges and output signals of both pressure sensors, the sensitivities of the inlet pressure sensor and the outlet pressure sensor are both 20, 000mv/MPa. Pressure data are collected by a data acquisition device with the sampling frequency of 2, 560Hz. The flow rate is tested by an electromagnetic flow meter, located at the outlet pipe close to the water tank.

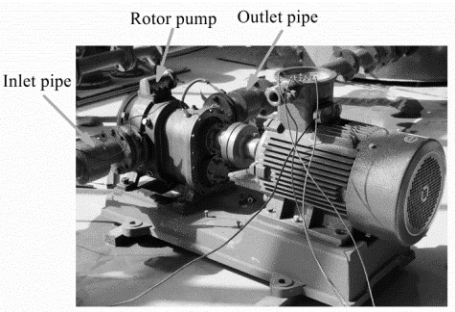

Fig. 2. Test configurations of the rotor pump

Working conditions

Generally speaking, the cavitation number is adopted to describe the cavitation state of rotor pumps, presented as Equation (12).

$$\sigma = \frac{p_{in} - p_v}{0.5\rho v_{in}^2} \tag{12}$$

The cavitation numbers chosen range from 1.89 to 6.96 in following tests. To study the effect of the inlet pressure on flow behavior of the rotor pump, both flow rates and inlet/outlet instantaneous pressures are monitored at different inlet pressures. During the experiment, the inlet pressures ranging from 67.44kPa to 20.69kPa are involved. Meanwhile, the pressure at the outlet changes with the inlet pressure, but the pressure difference between the inlet and the outlet is kept as a fixed value of 0.1MPa. It should be noted that in this work, the value of the inlet pressure is absolute pressure, while the value of the outlet pressure is gauge pressure.

Experimental results

Effect of inlet pressure on flow rates

Figure 3 displays the flow rates of the rotor pump (r=720r/min, p_{out}=0.1MPa) for different inlet pressures. It can be concluded that the flow rate decreases with the inlet pressure on the decrease. Moreover, with the inlet pressure decreasing, the flow rate has a more and more remarkable decrease. In this case, for the inlet pressure lower than 38.5kPa, the flow rate drops much more greatly than that higher than 38.5kPa. In addition, the flow rate falls about 3% compared with the original flow rate, when the pressure drops to 48.8kPa, which may be regarded as the critical pressure of the cavitation. When the inlet pressure decreases to 20.69kPa, the flow rate falls about 15% compared with the original flow rate. At this moment, the cavitation develops and affects the flow performance of the rotor pump greatly.

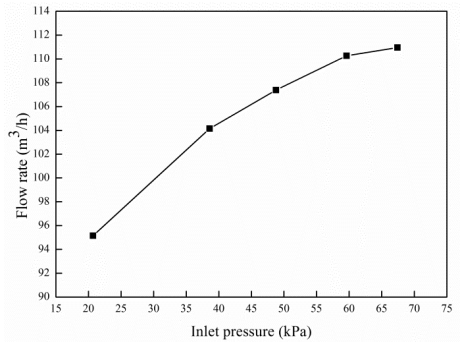

Fig. 3. Flow rates of the rotor pump (r=720r/min, p_{out}=0.1MPa) with various inlet pressures

Effect of inlet pressure on pressure fluctuation

Figure 4 reports the time histories of the inlet pressures and the corresponding frequency spectrums. The results show that the inlet pressure pulsates with the frequencies related to the rotating frequency f_n. For a higher inlet pressure (e.g. 67.44kPa), the highest amplitude occurs at the frequency of f_1=98.14 Hz and coincides with twice that of rotational frequency harmonics Zf_n (Z=4 in this case). In addition, other main frequencies include the frequencies of f_2=11.72Hz (f_n) and f_3=49.32Hz (Zf_n). The pressure pulsations at frequencies of f_1 and f_3 result from the inevitable unsteady discharge process of rotor pumps (Schiffer *et al*., 2013). However, as the inlet pressure decreases, the dominate frequency transforms from higher harmonics of rotational frequencies (e.g. $8f_n$) to lower frequencies (e.g. $4f_n$ and $2f_n$) gradually. The reason for the increase of the low-frequency pressure pulsation is the appearance of the pulsation frequencies of the cavitation bubbles, which starts to be a dominant factor during the development of the cavitation. The frequency is based on the time difference between the generation and the collapse of cavitation bubbles, which is always related to a lower frequency (Kjeldsen *et al.,* 2000).

The time histories of the outlet pressures and the corresponding frequency spectrums are shown in Figure 5. It can be found that the magnitude of the pressure pulsation increases gradually with the decreasing inlet pressures (Figures 5(a), 5(c), 5(e)), which may result from the appearance of the cavitation bubbles. As we all know, cavitation bubbles lead to an increase of the compressibility of the medium and a larger compressibility increases the unevenness of the flow rate, which is the basic reason for a larger pressure pulsation (Zhou, 2015). For the dominant frequencies of the outlet pressure (Figures 5(b), 5(d), 5(f)), as the inlet pressure decreases, the dominate frequency transforms from the higher harmonics of rotational frequency (e.g. $8f_n$) to the lower frequencies (e.g. $4f_n$ and $2f_n$) gradually, which is similar to the behavior of the frequency spectrum of the inlet pressure.

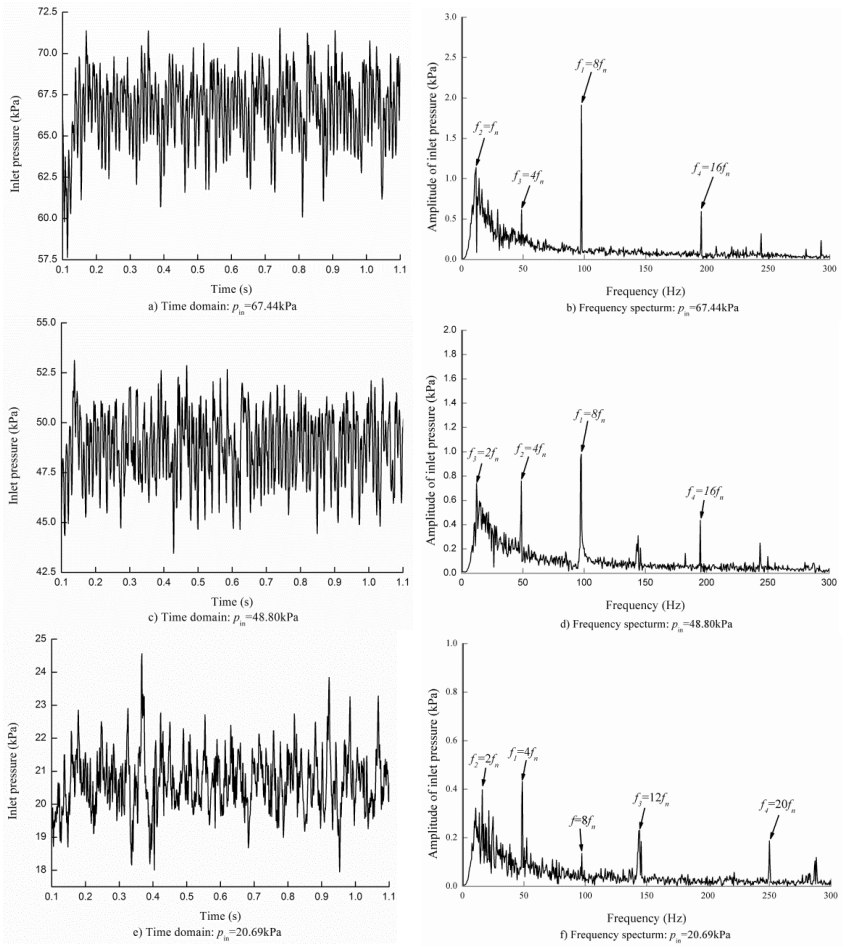

Fig. 4. Inlet pressure signals of the rotor pump (r=720r/min, p_{out}=0.1MPa)

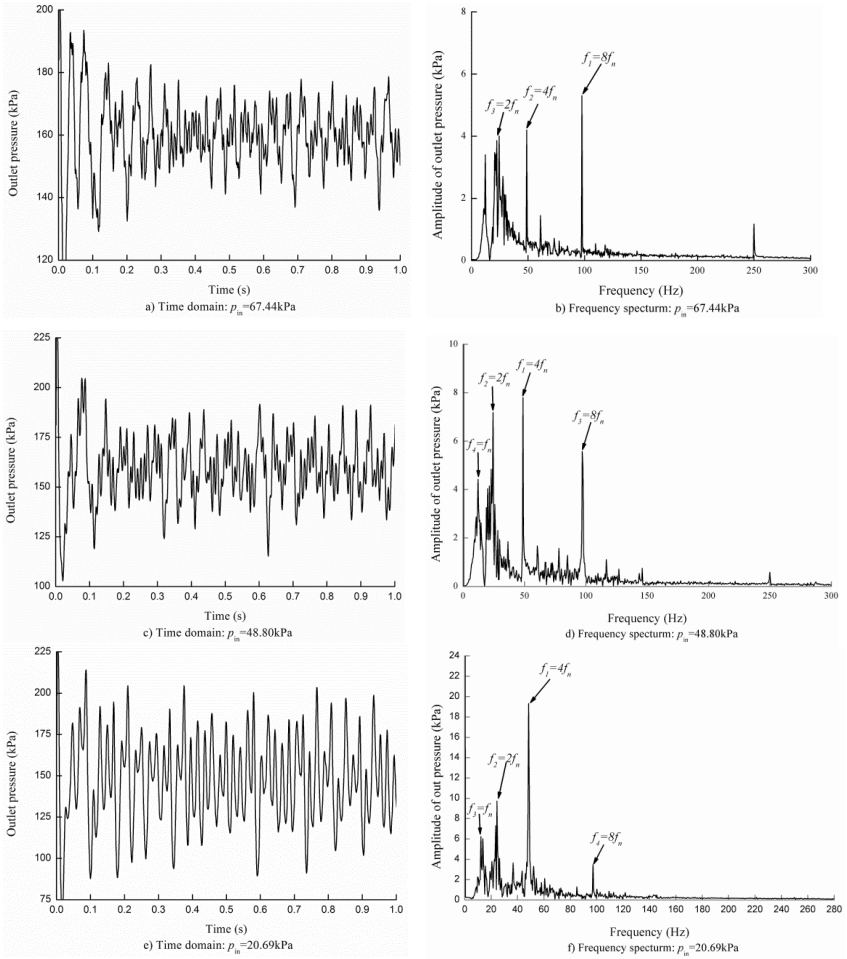

Fig. 5. Outlet pressure signals of the rotor pump (r=720r/min, p_{out}=0.1MPa)

NUMERICAL MODEL ON UNSTEADY CAVITATING FLOW IN ROTOR PUMPS

Computing geometry and grid

A simplified 2D model (Figure 6) is employed to analyze the cavitating turbulent flow of the rotor pump using the governing equations described above. The main geometrical parameters of the pump are presented in Table 1. For the pump, the gap size between two rotors is 0.1mm and the gap size between rotors and pump case is 0.16mm. The model is based on the computer package Fluent, which has been confirmed accurate enough to discuss the effect of the main geometrical and working conditions on the flow characteristics of rotor pumps (Campo *et al*., 2012). It should be noted that the calculated flow rate should be multiplied by the rotor width (L) when it is compared with the experimental data.

Table 1. Main geometrical parameters of the test pump

Parameters	Value
Diameter of the rotors	86.9mm
Distance between centers of rotors	125mm
Number of impeller	4
Theoretical volumetric capacity	21.63m^2/rev

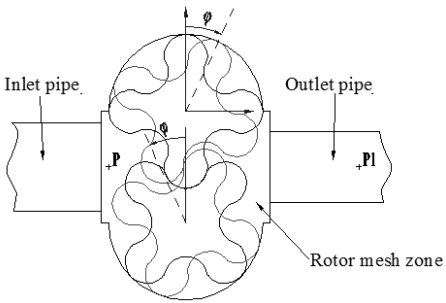

Fig. 6. Geometrical model of the rotor pump

The synchronous motion of the two rotors is analyzed by dynamic mesh method and their rotational speeds are set through the user defined functions (UDF). An approach of dynamic mesh based on a Laplacian smoothing algorithm with local re-meshing is employed, which can produce smaller numerical errors, when the cavitation is mentioned (Campo *et al*., 2014). In addition, parameters for local re-meshing play a significant role on the grid quality in the process of mesh updating. A mesh analysis of two parameter combinations (Table 2) defining mesh updating is carried out. There are three parameters for Fluent to evaluate each cell and mark it for remeshing, including the minimum length scale, the maximum length scale and the maximum cell skewness. If it meets one or more of the criteria related to the three parameters, Fluent updates the mesh automatically. Seeing that shortening the difference between the minimum length scale and the maximum length scale, and reducing the maximum cell skewness may obtain a better-quality grid, two parameter combinations (A and B) are adjusted based on the default parameter combination and adopted for mesh analysis. The calculated outlet flow rates and the average mesh skewness are plotted in Figure 7. It can be indicated that the flow rates obtained by combinations A and B are similar to each other. However, the mesh skewness of combination B is much smaller than that of combination A. Thus, parameter combination B is adopted to describe the mesh updating. Its original mesh (φ=0°) and the mesh after updating (φ=10°) are both shown in Figure 8. In addition, the element and node numbers of the model are 323,015 and 164,030, respectively.

Table 2. Parameter combinations used for defining mesh updating in Fluent

Parameters	Defaults	A	B
Minimum length scale (mm)	0.0964	0.1	0.2
Maximum length scale (mm)	1.5	1.6	0.6
Maximum cell skewness	0.727	0.6	0.5

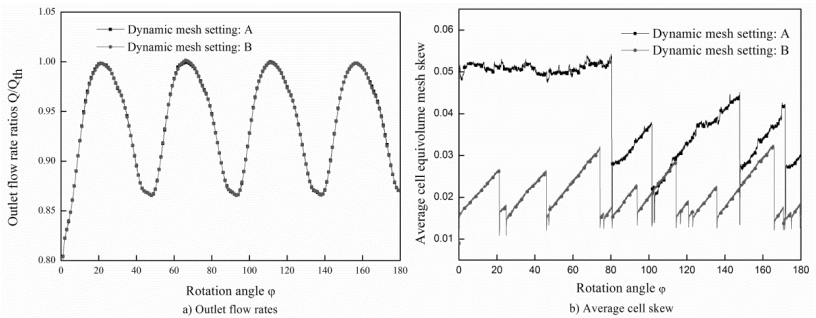

Fig. 7. Comparison of numerical results by parameter combinations A and B (r=720r/min, p_{out}=0.1MPa)

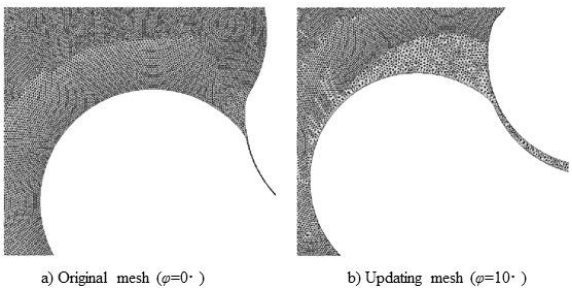

Fig. 8. Grid of the rotor domain

Boundary and initial conditions

The outlet and inlet boundary conditions are set as pressure outlet and pressure inlet, respectively. The values are determined by the actual pressures. In order to guarantee the steady of the calculation, the flow of the rotor pump without cavitation is calculated firstly and the results are regarded as the initial conditions for the calculation with cavitation.

Determination of cavitation model

Given that the parameters of Zwart-Gerber-Belamri cavitation model are easy to adjust, this model is employed to describe the mass transfer between two phases. There are four parameters in this model and they are bubble diameter R_b, nucleation site volume fraction r_{nuc}, evaporation coefficient F_{vap} and condensation coefficient

F_{con}. Where, nucleation site volume fraction α_{nuc} is generally given by the Bunsen coefficient, which represents the ratio of the volume of gas and the volume of fluid at atmospheric conditions (Campo *et al*., 2012). In this case, the Bunsen coefficient for water is 0.0005. The condensation coefficient F_{con} has a little effect on cavitation and its default value (0.01) is adopted. The flow rates of the rotor pump for different bubble diameters R_b and different evaporation coefficients F_{vap} are indicated in Figure 9. This case corresponds to a rotational speed of 720r/min and an inlet pressure of 67.44kPa. Numerical results show that the main frequency of the inlet pressure (61.74kPa) is $8f_n$ (Figure 11(b)). Therefore, the magnitudes of the pressure pulsations under the same frequency ($8f_n$) are adopted for comparison. Generally, the amplitude of the pressure fluctuation is adopted to describe the magnitude of pressure fluctuation, which is defined as half of the difference between the maximum value and the minimum value. Experimental results show that the amplitude of the flow rate pulsation is approximately $10m^3/h$ and the amplitude of the inlet pressure under the same frequency of $8f_n$ is approximately 2kPa (Figure 4(a)). Numerical results demonstrate that for the combination of R_b=0.01mm and F_{vap} =0.4, the amplitude of the flow rate pulsation is $8.36m^3/h$ (Figure 9(a)) and the amplitude of the inlet pressure under the same frequency of $8f_n$ is 1.84kPa (Figure 9(b)), presenting that numerical results are consistent with the experimental results and the combination of R_b=0.01mm and F_{vap} =0.4 adopted in this work is reasonable for analysis.

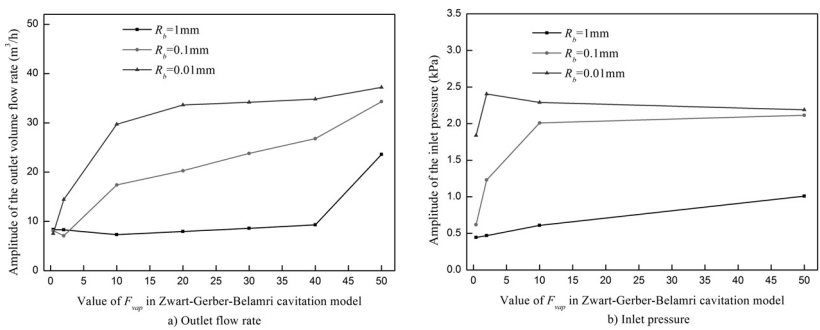

Fig. 9. Amplitudes of outlet flow rates and inlet pressures under the same frequency of $8f_n$ by different cavitation model settings

Validation of numerical model

Flow rates obtained by the above 2D model are compared with the experimental data (Liu *et al*., 2015) with a pressure difference of 0.1MPa (Figure 10). The results show that the calculated flow rates with a pressure difference of 0.1MPa agree well with the experimental data, indicating that the 2D model is reasonable for working conditions with a low pressure difference (e.g. 0.1MPa). Thus, the pressure difference of 0.1MPa is adopted to discuss the influence of the inlet pressure on flow characteristics of the rotor pump in following.

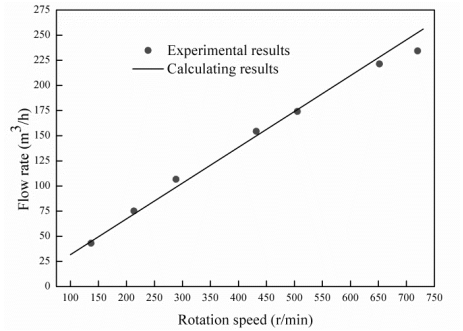

Fig. 10. Comparison of flow rates between numerical and experimental results (p_{out}=0.1MPa, L=160mm)

Then the pressure fluctuation of the inlet pressure and its frequency spectrum for single-phase flow and cavitating flow are compared in Figure 11. It can be seen that the amplitude of pressure pulsation obtained by cavitating flow based on the mixture model (1.84kPa, Figure 11(a)) agrees much better with experimental data (2kPa, Figure 4(a)) than that by single-phase flow model (0.82kPa, Figure 11(a)). The results of spectrum analysis indicate that the largest contribution of the pressure pulsations mainly stems from $8f_n$, similar to the experimental data. However, some lower harmonic frequencies of the rotating frequency in the test pump are not obtained through numerical studies. This is probably because these lower frequencies result from eccentricities and other geometrical imperfections of the rotating rotors (Casoli *et al.,* 2005, Schiffer *et al*., 2013).

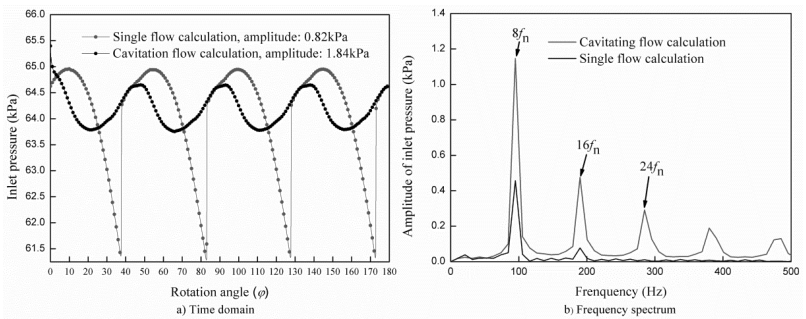

Fig. 11. Inlet pressure fluctuation for single phase and cavitation flow calculation (r=720r/min, p_{out}=0.1MPa)

Taking the case with the inlet pressure of 20.69kPa and the rotational speed of 720r/min as an example (σ=3.09), the ratio of the volumetric flow rate Q and theoretical flow rate Q_{th} at the inlet and outlet with and without cavitation are shown in Figure 12. When the cavitation is not included, the flow rates of the inlet and the outlet do not present remarkable differences. However, the flow rates have a big difference between

the inlet and the outlet, when cavitation is taken into consideration. Exactly speaking, for the inlet, cavitation boosts the amplitude and the average value of the flow rates, while it has a little effect on the outlet flow rates. This is because that cavitation appears at the suction side of the pump (Figure 17) and the cavities increase the compressibility of the medium, leading to a larger instability of the inlet flows. However, when the medium gradually flows into the following chambers, some bubbles carried by the medium flow back to the previous chamber and start to collapse. Finally, the flow becomes more and more steady, when the medium flows into the outlet pipe of the pump, which affects the outlet flow slightly. However, it should be noted that the peak of the outlet flow is not very obvious, which means the cavitation plays an inhibited role on outlet flows of the rotor pump.

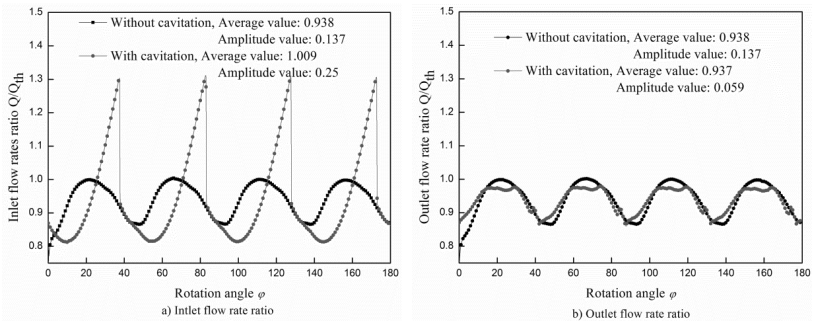

Fig. 12. Flow rates with and without cavitation

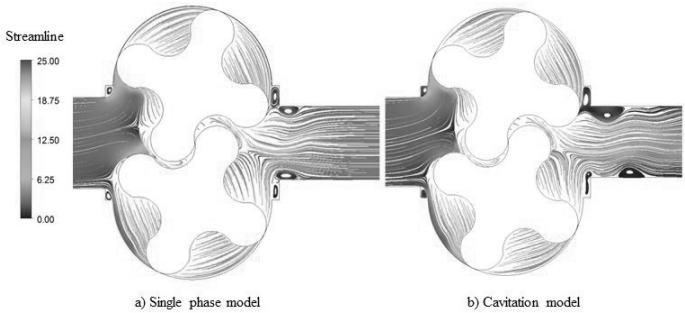

Fig. 13. Streamlines of the rotor pump(r=720r/min, p_{in}=20.69kPa)) (φ=20°)

Figure 13 shows the streamline distributions in the rotor pump using single-phase model and cavitation model. It can be found that compared with the sing-phase model, there are more obvious vortexes and a larger velocity gradient, when the cavitation is included, which induces the instability of the flow.

EFFECT OF INLET PRESSURE ON FLOW CHARACTERISTICS OF ROTOR PUMP

Effect of inlet pressure on flow rate ratios

The flow rate ratios of the inlet and the outlet with the rotation speed of 960r/min for various inlet pressures are shown in Figure 14. It can be found that with the inlet pressure p_{in} on the decrease, as a whole, the peak of the volumetric ratio decreases at the inlet, but increases at the outlet. For the inlet flow rate ratio, the pulsation period becomes longer for a lower inlet pressure (e.g. 20.69kPa) than that for a higher inlet pressure (e.g. 80.0kPa). Moreover, the peak of the inlet flow rate ratio offsets backward as the inlet pressure decreases. This is because that the vapor bubbles produced by cavitation play an inhibited role on the suction capability of the rotor pump. Once lots of vapor bubbles appear, the vapor is evacuated by the pump firstly and the suction time for water delays. For the flow rate ratio at the outlet, its amplitude changes slightly at the most time of the period as the inlet pressure decreases. However, there is a slight increase at the peak of the flow rate ratio (Figure 14 (b)), when the inlet pressure drops to a lower value (e.g. 38.575kPa). Regarding to the peak of the outlet flow rate ratio, it does not display any delay with the drop of the inlet pressure. This is probably because cavitation has a limited influence on outlet flows, which has been discussed in the section of ***Validation of numerical model***.

Figure 15 shows the comparison of the velocity contours of the rotor pump at different inlet pressures. It can be seen that, when the inlet pressure (cavitation number) drops, a greater velocity gradient can be found at the meshing zone of the rotors. This also explains why the flow performance of the rotor pump becomes unsteady with the decline of the inlet pressure.

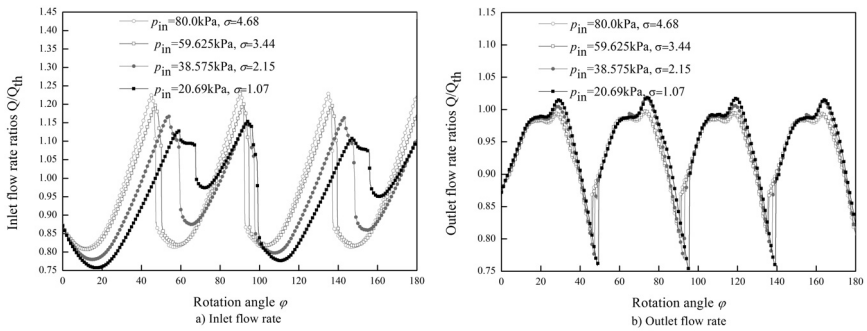

Fig. 14. Flow rate ratios of the rotor pump under different inlet pressures (r=960r/min)

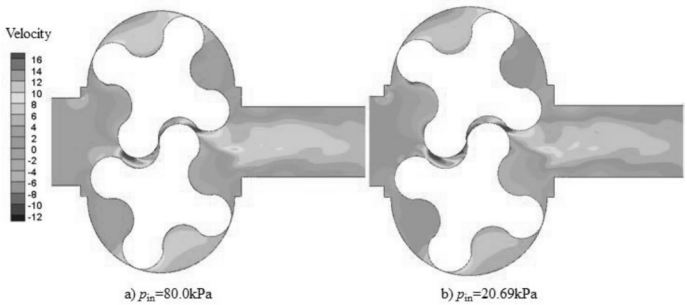

Fig. 15. Velocity contours of rotor pump at different inlet pressures (r=960r/min)

Effect of inlet pressure on volume fractions of vapor phase

The volume fraction of the vapor phase is adopted to describe the cavitation degree and the results are presented in Figure 16. It can be demonstrated that the volume fraction of the vapor phase has a remarkable increase, when the inlet pressure decreases from 59.625kPa to 38.575kPa. In addition, the vapor phase shows a remarkable periodicity, when the inlet pressure is relatively high (e.g. 59.625kPa) and the period of the vapor fraction prolongs, when the inlet pressure drops to a lower value (e.g. 38.575kPa), which is similar to the behavior of the inlet flow rate. However, the vapor fraction becomes unsteady, when the inlet pressure drops to 20.69kPa, which means the cavitation develops greatly at this inlet pressure.

Figure 17 shows the volume fraction distribution of cavitation bubbles under different inlet pressures. It can be seen that cavities are mainly located at the regions of the contact point. Meanwhile, the area of the vapor phase expends and the fraction of the vapor phase increases, when the inlet pressure decreases.

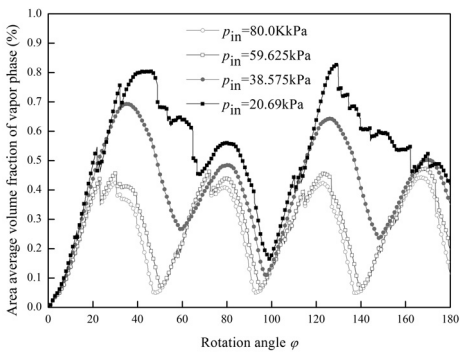

Fig. 16. Average volume fraction of vapor phase under different inlet pressures (r=960r/min)

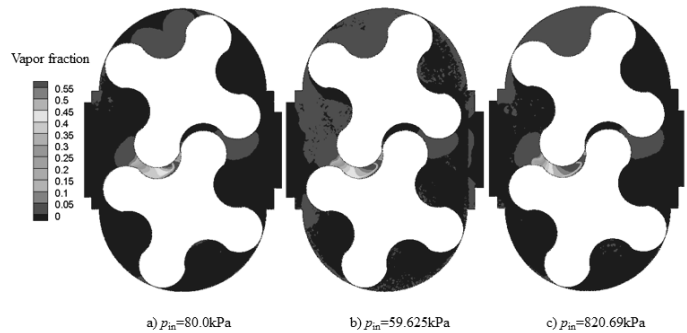

Fig. 17. Volume fraction distribution of cavitation bubbles at different inlet pressures (r=960 r/min, φ=25°)

Effect of inlet pressure on pressure fluctuations

Figure 18 shows the pressure fluctuations of Point P at the suction side and Point P1 at the discharge side (Figure 6) of the rotor chamber with various inlet pressures. It can be found that pressures at the suction and discharge sides both present a sudden increase at a certain moment. For a high inlet pressure (e.g. 80kPa), the pressure mutation occurs approximately, when the two rotors are fully engaged with each other. However, the time for the pressure mutations delays with the decreasing inlet pressures. Exactly speaking, for the pressure fluctuation of Point P (the suction side), the time delayed prolongs greatly, when the inlet pressure decreases to a small value (e.g. 38.575kPa), which also results from the inhibited role of the vapor bubbles. For the pressure fluctuation of Point P1 (the discharge side), the time delayed is shorter than that of Point P. The reason for this phenomenon may be the same as that for outlet flow rates. In addition, the amplitude of the outlet pressure mutation increases with the decreasing inlet pressures, which agrees well with the experimental results.

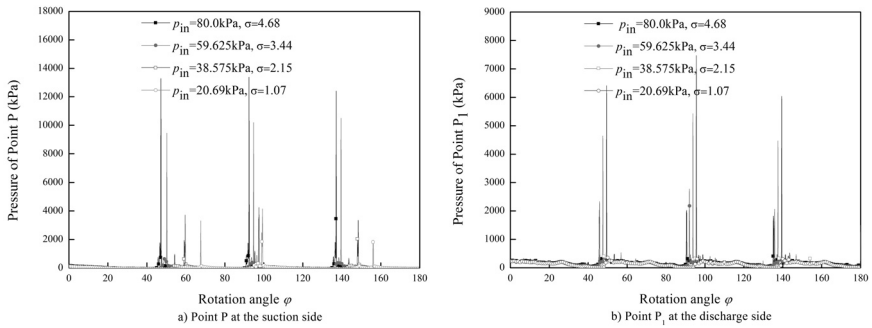

Fig. 18. Pressure fluctuations of Points P and P_1 at different inlet pressures

CONCLUSION

In this work, the effect of the inlet pressure on the unsteady cavitating flows in a rotor pump is investigated through experimental and numerical studies. The following conclusions are drawn from this study.

(1) As the inlet pressure decreases, the dominate frequency transforms from the higher harmonics of rotational frequency ($2 \cdot Zf_n$) to some lower frequencies (Zf_n and $1/2 \cdot Zf_n$, et.al).

(2) Numerical results of the flow performance in the rotor pump based on the cavitation model agree much better with experimental data than that by single phase model.

(3) The flow rates have a big difference between the inlet and the outlet, when cavitation is taken into consideration. Exactly speaking, for the inlet, cavitation boosts the amplitude and the average value of the flow rates, while it has a little effect on outlet flow rates.

(4) The volumetric ratio decreases at the inlet but increases at the outlet with the inlet pressure on the decrease. Moreover, the peak of the inlet flow rate ratio offsets backward as the inlet pressure decreases but the peak of outlet flow rate ratio does not display any delay.

(5) The period of the inlet flow rate ratio, as well as the volume fraction of the vapor phase, is longer for a lower inlet pressure than that of a higher inlet pressure.

(6) Both the pressures at suction and discharge sides present a sudden increase at a certain moment. For a high inlet pressure, the pressure mutations occur, when the two rotors are fully engaged with each other, while the time for pressure mutation delays for a low inlet pressure.

REFERENCES

Brennen, C.E. 1995. Cavitation and bubble dynamics, Oxford University, Press, Oxford.

Campo, D., Castilla, R. & Codina, E. 2012. Analysis of the suction chamber of external gear pumps and their influence on cavitation and volumetric efficiency. Universitat Politècnica de Catalunya, Spain.

Campo, D., Castilla, R., Raush, G.A., Gamez-Montero, P.J.G. & Codina, E. 2012. Numerical analysis of external gear pumps including cavitation. Journal of Fluids Engineering, **134** (081105):1-12.

Campo, D., Castilla, R., Raush, G.A., Gamez-Montero, P.J.G. & Codina, E. 2014. Pressure effects on the performance of external gear pumps under cavitation. Proceedings of the Institution of Mechanical Engineers, Part C: Journal of Mechanical Engineering Science, **228**(16):2925-2937.

Casoli, P., Vacca, A. & Franzoni, G. 2005. A numerical model for the simulation of external gear pumps. 6th JFPS international symposium on fluid power, Tsukuba, Japan.

Castilla, R., Gamez-Montero, P.J. & Erturk, N. 2010. Numerical simulations of turbulent flows in the

suction chamber of a gear pump using deforming mesh and mesh replacement. International Journal of Mechanical Sciences, 52(10):1334-1342.

Erturk, N., Vernet, A. & Castilla, R. 2011. Experimental analysis of the flow dynamics in the suction chamber of an external gear pump. International Journal of Mechanical Sciences, 53(2):135-144.

Ertürk, N., Vernet, A., Ferré, J.A. Castilla, R. & Codina, E. 2008. Analysis of the turbulent flow of an external gear pump by time resolved particle image velocimetry. 14th International Symposium on Applications of Laser Techniques to Fluid Mechanics, Lisbon, Portugal.

Fluent A. 14.5, Theory Guide. 2012. ANSYS Inc.

Huang, S., Su, X.S., Guo, J. & Yue, L. 2014. Unsteady numerical simulation for gas-liquid two-phase flow in self-priming process of centrifugal pump. Energy Conversion and Management, 85:694-700.

Huang, Z.F. & Liu, Z.X. 2009. Numerical study of a positive displacement blower. Proceedings of the Institution of Mechanical Engineers, Part C: Journal of Mechanical Engineering Science, 223(10):2309-2316.

Kjeldsen M., Arndt R.E.A. & Effertz M. 2000. Spectral characteristics of sheet/cloud cavitation. Journal of Fluids Engineering, **122**(3): 481-487.

Liu, H.C., Tong, S.H. & Yang, D.C.H. 2000. Trapping-free rotors for high-sealing lobe pumps. Journal of Mechanical Design-Transactions of the ASME, **122**(12): 536-542.

Liu S. H., Zhang, L., Nishi, M. & Wu, Y.L. 2009. Cavitating turbulent flow simulation in a Francis turbine based on mixture model. Journal of Fluids Engineering, **131**(5):051302.

Liu, Y.Y., Wang, L.Q. & Zhu, Z.C. 2014. Numerical study on flow characteristics of rotor pumps including cavitation. Proceedings of the Institution of Mechanical Engineers, Part C: Journal of Mechanical Engineering Science, 229(14):2626-2638.

Mejri, M., Bakir, F., Rey, R. & Belamri, H. 2006. Comparison of computational results obtained from a homogeneous cavitation model with experimental investigations of three inducers. Journal of Fluids Engineering, **12**(28):1308-1323.

Schiffer, J., Benigni, H. & Jaberg, H. 2013. Development of a novel miniature high-pressure fuel pump with a low specific speed. Proceedings of the Institution of Mechanical Engineers, Part D: Journal of Automobile Engineering, **227**(7): 997-1006.

Totten, G.E., Sun, Y.H., Lin, X. & Bishop, R.J. 1998. Hydraulic system cavitation: A review. SAE Technical Paper Series: No. 982036.

Zwart, P.J., Gerber, A.G. & Belamri, T. 2004. A two-phase flow model for predicting cavitation dynamics. 5th International Conference on Multiphase Flow, Yokohama, Japan.

Zhang, L.X. & Khoo, B.C. 2014. Dynamics of unsteady cavitating flow in compressible two-phase fluid. Ocean Engineering, 87:174-184.

Zhang, Y., Luo X.W., Ji Bi., Liu S.H., Wu Y.L. & Xu H.Y. 2010. A thermodynamic cavitation model for cavitating flow simulation in a wide range of water temperatures. Chinese Physics Letters, **27**(1): 016401.

Zhou, J.J. 2015. Study on cavitation in multi-connected volumes and its effects on the operation of gear pumps, Ph.D. thesis Beijing Institute of Technology, P.R.

Submitted: 3/5/2015
Revised: 29/11/2015
Accepted: 30/12/2015